https://doi.org/10.5194/egusphere-2026-1315
Preprint. Discussion started: 8 April 2026

Inferring European Fossil Fuel CO_2 Emissions using TROPOMI NO_2 Data and Sector-Based NO_x:CO_2 Emission Ratios

Chlöe N. Schooling[1], Liang Feng[1], Ingrid Super[2], and Paul I. Palmer[1,3]

[1]School of GeoSciences, University of Edinburgh, Edinburgh, United Kingdom
[2]Department of Air Quality and Emissions Research, TNO, P.O. Box 80015, 3508 TA Utrecht, the Netherlands
[3]National Centre for Earth Observation, University of Edinburgh, Edinburgh, United Kingdom

Corresponding author: Chlöe N Schooling (cschooli@ed.ac.uk) and Paul I Palmer (pip@ed.ac.uk)

Abstract. Accurate monitoring of fossil fuel CO_2 ($ffCO_2$) emissions is essential for tracking climate mitigation, yet natural carbon-cycle fluxes often obscure human-induced signals in atmospheric observations. This study presents a satellite-driven data assimilation framework that uses nitrogen oxides (NO_x = NO + NO_2) − short-lived trace gases co-emitted with CO_2 − to estimate $ffCO_2$ emissions. We estimate European NO_x emissions for 2021 by assimilating TROPOMI NO_2 observations into an Ensemble Kalman Filter (EnKF) framework, optimised within the GEOS-Chem atmospheric transport model. We use a computationally efficient offline treatment of NO_x chemistry, enabling large-ensemble inversions while retaining sensitivity to changes in photochemistry. Assimilating these data leads to a systematic reduction in the state vector uncertainty, with a mean ensemble-based error reduction of 4.2–5.7%, and an overall improvement in model agreement with observations that corresponds to an annual correlation increase, Δr =0.12. By leveraging sector-specific NO_x:CO_2 emission ratios, we translate our posterior NO_x flux estimates into improved $ffCO_2$ estimates that capture enhanced seasonal variability. Our inferred $ffCO_2$ emissions exhibit elevated values in autumn and winter, spatially concentrated over major source regions and consistent with surface temperature variability. Independent evaluation against *in situ* measurements confirms significant improvements in mean error statistics. While OCO-2 CO_2 column data remain dominated by biogenic signals, our NO_2-driven approach successfully isolates the fossil fuel component. This study demonstrates the potential of ensemble data assimilation and reduced-complexity chemistry to provide physically consistent constraints on European $ffCO_2$ estimates, establishing a vital foundation for future joint NO_2–CO_2 inversion systems.

1 Introduction

Fossil fuel CO_2 ($ffCO_2$) emissions are the primary driver of anthropogenic climate change. Accurately monitoring these emissions is essential for tracking progress toward national mitigation goals, yet it is complicated by the difficulty of isolating fossil fuel signals from large, seasonally varying biogenic fluxes. Top-down atmospheric inversions offer a way to improve emission estimates of $ffCO_2$, but they are limited by observational constraints and the inability to directly differentiate anthropogenic CO_2 from natural sources.

https://doi.org/10.5194/egusphere-2026-1315
Preprint. Discussion started: 8 April 2026

Studies are increasingly using atmospheric observations of trace gases co-emitted during combustion processes to infer $ffCO_2$ emissions (Meijer et al., 1996; Suntharalingam et al., 2004; Palmer et al., 2006; Lopez et al., 2013; Wenger et al., 2019; Super et al., 2020b; Miyazaki and Bowman, 2023). Nitrogen oxides (NO_x) are a leading candidate tracer to help infer $ffCO_2$ because they originate almost exclusively from combustion and have a short atmospheric lifetime so that fresh emissions can be readily identified. High-resolution satellite observations of NO_2, such as those from TROPOMI, provide detailed patterns of emission activity. These measurements have been extensively used to infer NO_x emissions, either through mass balance methods (de Foy et al., 2015; Visser et al., 2019; Sun, 2022), comprehensive atmospheric inversions that account for transport and chemistry (Stavrakou et al., 2008; Gu et al., 2014; Itahashi et al., 2019; Plauchu et al., 2024; Kong et al., 2025), or hybrid approaches that combine elements of both (Qu et al., 2017, 2020). By applying sector-dependent emission ratios, it is then possible to infer spatial patterns of $ffCO_2$ from these NO_x emission estimates (Berezin et al., 2013; Lopez et al., 2013; Goldberg et al., 2019, 2024; Jia et al., 2025). Preliminary studies have assessed the ability of using synthetic atmospheric observations of both NO_2 and CO_2 in tandem to assess methodologies for more robust estimates of $ffCO_2$ flux (Kuhlmann et al., 2021; Kaminski et al., 2022; Santaren et al., 2025).

However, such a tracer-based approach is subject to substantial uncertainties. A key limitation is the uncertainty associated with the CO2 and NOx emission ratios, which vary by sector, fuel type, combustion technology, and emission control strategies (Jiang et al., 2010; Wang et al., 2025; Super et al., 2020a). Additional challenges include errors in atmospheric transport modelling, uncertainties in the representation of chemical processes controlling NO_x lifetimes, sparse and inhomogeneous observational coverage, and the difficulty of accurately estimating background concentrations (Peylin et al., 2013; Andrew, 2020). These factors complicate the interpretation of NO_2 columns and the propagation of information from observed concentrations back to surface emissions and, ultimately, to $ffCO_2$ fluxes. Data assimilation frameworks such as the Ensemble Kalman Filter (EnKF) provide a powerful means of addressing some of these challenges by explicitly representing and propagating uncertainties in emissions, chemistry, transport, and observations.

We present a methodology that uses TROPOMI NO_2 observations within an Ensemble Kalman Filter (EnKF) framework to infer daily NO_x emission estimates over Europe during 2021. Our approach uses the GEOS-Chem model with a novel, lightweight offline NO_x chemistry module, extending the work of Schooling et al. (2025). By embedding this reduced-complexity chemistry within an ensemble data assimilation system, we achieve a computationally efficient pathway for satellite-derived $ffCO_2$ estimation. This framework establishes a scalable foundation for future joint inversions of NO_2 and CO_2.

In the next section, we describe the data and methods, including TROPOMI NO_2 data, the GEOS-Chem atmospheric chemistry transport and its configuration used for the experiments we report here that includes our offline NO_x chemistry module, and the coupled ensemble Kalman filter. We also include details about the sector-based NO_x:CO_2 emission ratios used to translate our posterior NO_x emission estimates into $ffCO_2$ emission estimates. In section 3, we describe our results. We conclude our study in section 4.

https://doi.org/10.5194/egusphere-2026-1315
Preprint. Discussion started: 8 April 2026

2 Data and methods

2.1 Atmospheric NO_2 Observations

We use satellite observations of NO_2 from the TROPOspheric Monitoring Instrument (TROPOMI) to constrain anthropogenic NO_x emissions over Europe. TROPOMI is a push-broom imaging spectrometer aboard Copernicus Sentinel-5 Precursor (S5P), launched in October 2017. S5P operates in a sun-synchronous Low-Earth Orbit at an altitude of approximately 824 km, with an ascending node local equator-crossing time of 13:30. TROPOMI has an across track swath of 2,600 km, resulting in a daily global coverage. The nadir spatial resolution for NO_2 was initially 7×3.5 km^2 and was further refined to 5.5×3.5 km^2 in August 2019. The NO_2 retrievals use the UV/Vis spectral range (405−465 nm), with a reported single measurement uncertainty of 0.7×10^{15} molec/cm^2, subject to clear-sky scenes (Veefkind et al., 2012; van Geffen et al., 2022). For our study, we use v2.4.0 of the Sentinel-5P TROPOMI Level-2 NO_2 data for the full year of 2021. We consider measurements that have a quality assurance value $\mathtt{qa} \geq 0.75$ to remove low-quality pixels (van Geffen et al., 2022).

To evaluate the NO_x posterior emission estimates inferred from TROPOMI NO_2 column data, and the corresponding $ffCO_2$ estimates, we use independent atmospheric NO_2 and CO_2 measurements.

We use satellite observations of column-averaged CO_2 retrieved from the NASA Orbiting Carbon Observatory (OCO-2) to evaluate the influence of our posterior $ffCO_2$ emission estimates on the total column. We acknowledge fresh $ffCO_2$ emissions represent at most a few percent of the column quantity so that distinguishing the anthropogenic signal from the natural carbon cycle and background concentrations becomes a significant observational challenge. Despite this, the high precision of OCO-2 measurements (0.5ppm (Jacobs et al., 2024)) allows us to detect subtle enhancements in the total column over major industrial regions and urban centres (Schwandner et al., 2017; Ye et al., 2020). We use the Level 2 Lite Full Physics product retrieved using the Atmospheric CO_2 Observations from Space (ACOS) algorithm, version 10. These data provide bias-corrected, quality-screened XCO_2 retrievals with a footprint of approximately 1.3×2.25 km^2, acquired in nadir with a local overpass time of 13:30. Due to OCO-2's narrow ∼10 km swath and strict cloud filtering, spatial coverage is sparse. For consistency with our NO_2 filtering criterion, we select only high-quality retrievals with a quality assurance value $\mathtt{qa} \geq 0.75$. Both satellite datasets were resampled to the GEOS-Chem nested model resolution of 0.25° (latitude) × 0.3125° (longitude); the model is described below. Figure 1a shows the proportion of European grid points covered per day and per month for TROPOMI and OCO-2 (Fig. 1a). Generally coverage is highest during summer months. To ensure accurate comparison with observations, we interpolate the satellite averaging kernels onto the 47 vertical levels of the model to compute vertically sensitive model column densities.

We also used in situ measurements of NO_2 and CO_2 collected across Europe (Fig. 1b). We use NO_2 data from the European Environment Agency (EEA) air quality network (European Environment Agency and Heisig, 2025), including 202 sites across Europe that had at least 100 days of coverage in 2021. EEA data are processed using standardised quality filtering procedures, and data are reported with a mean uncertainty of 4 μg/m^3 across rural and urban background areas (Horálek et al., 2023). We also used in situ measurements of CO_2 from multiple ground-based monitoring networks across Europe, including the Integrated Carbon Observation System (ICOS) (ICOS RI et al., 2025), the National Oceanic and Atmospheric Administration

https://doi.org/10.5194/egusphere-2026-1315
Preprint. Discussion started: 8 April 2026

(NOAA) network (NOAA Global Monitoring Laboratory and Group, 2025), and the UK's Department for Energy Security and Net Zero (formerly DECC) sites (Stanley et al., 2018).

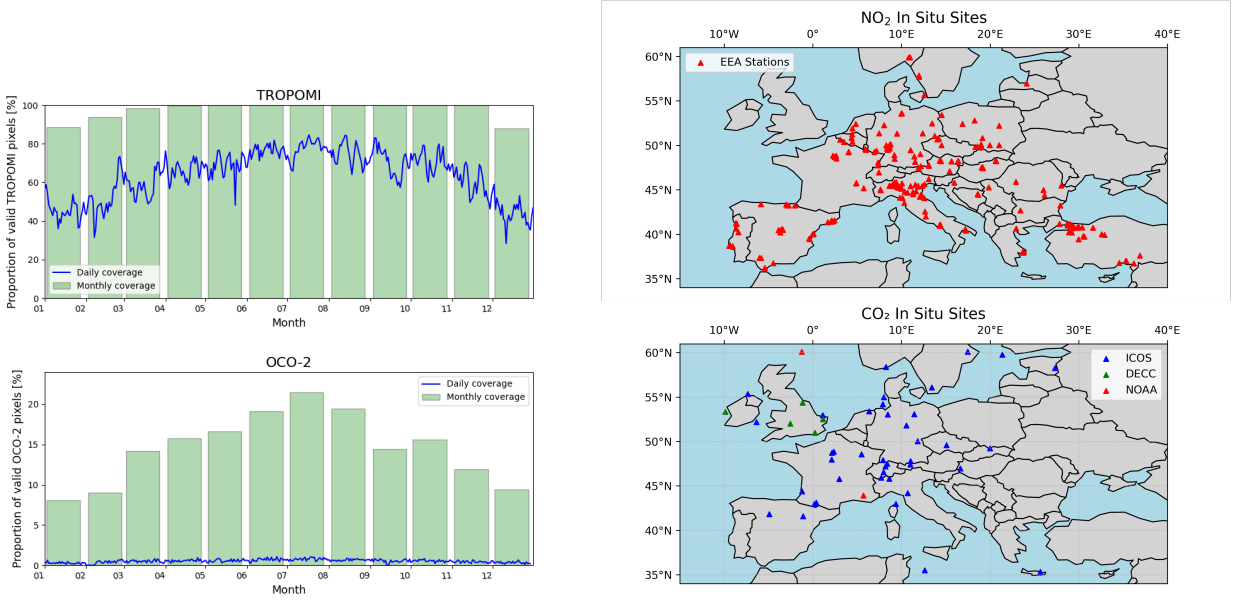

Figure 1. (a) The fractional daily and monthly European coverage of TROPOMI NO_2 and OCO-2. Coverage is defined as the fraction of GEOS-Chem model grid cells across the European domain that receive at least one clear-sky TROPOMI observation within the specified time period. Thus, 100% daily coverage means every model grid was observed at least once during the period (day or month). (b) Map of the 202 EEA in situ NO_2 stations and 47 in situ CO_2 measurement sites, which include 40 ICOS, 5 DECC, and 2 NOAA.

2.2 The GEOS-Chem atmospheric chemistry transport model

We use the nested version of the GEOS-Chem atmospheric chemistry transport model (version 14.4.3) (Bey et al., 2001). The model is driven by offline meteorological fields from the GEOS-FP dataset provided by NASA's Global Modeling and Assimilation Office (GMAO), using the native horizontal resolution of 0.25°x0.3125°, 47 vertical levels (grouped from the native 72 levels), and 3-hourly temporal resolution. Our simulations use an adapted tagged CO_2 model configuration that includes a lightweight offline treatment of NOx chemistry, described below.

The nested model is centred over mainland Europe (32.75 to 61.25°N, -15 to 40 °E). Lateral boundary conditions to the European domain were created from a consistent global GEOS-Chem model run at 4°×5°, with three-hourly output fields. The nested model was run with a 5-minute transport timestep and 10-minute chemistry timestep.

Prior combustion emissions of NO_x and CO_2 are taken from the CAMS-REG v8.1 emissions inventory at 0.05°x0.1° resolution (Fig. 2) (Kuenen et al., 2022). Temporal variability in emissions (monthly, daily, hourly) is represented using sector-based scaling factors provided by TNO (Netherlands Organisation for Applied Scientific Research) (Figure 2). Combustion sectors include public power, industry, road transport, ships, aviation, off-road machinery, and other combustion sources. Emissions

https://doi.org/10.5194/egusphere-2026-1315
Preprint. Discussion started: 8 April 2026

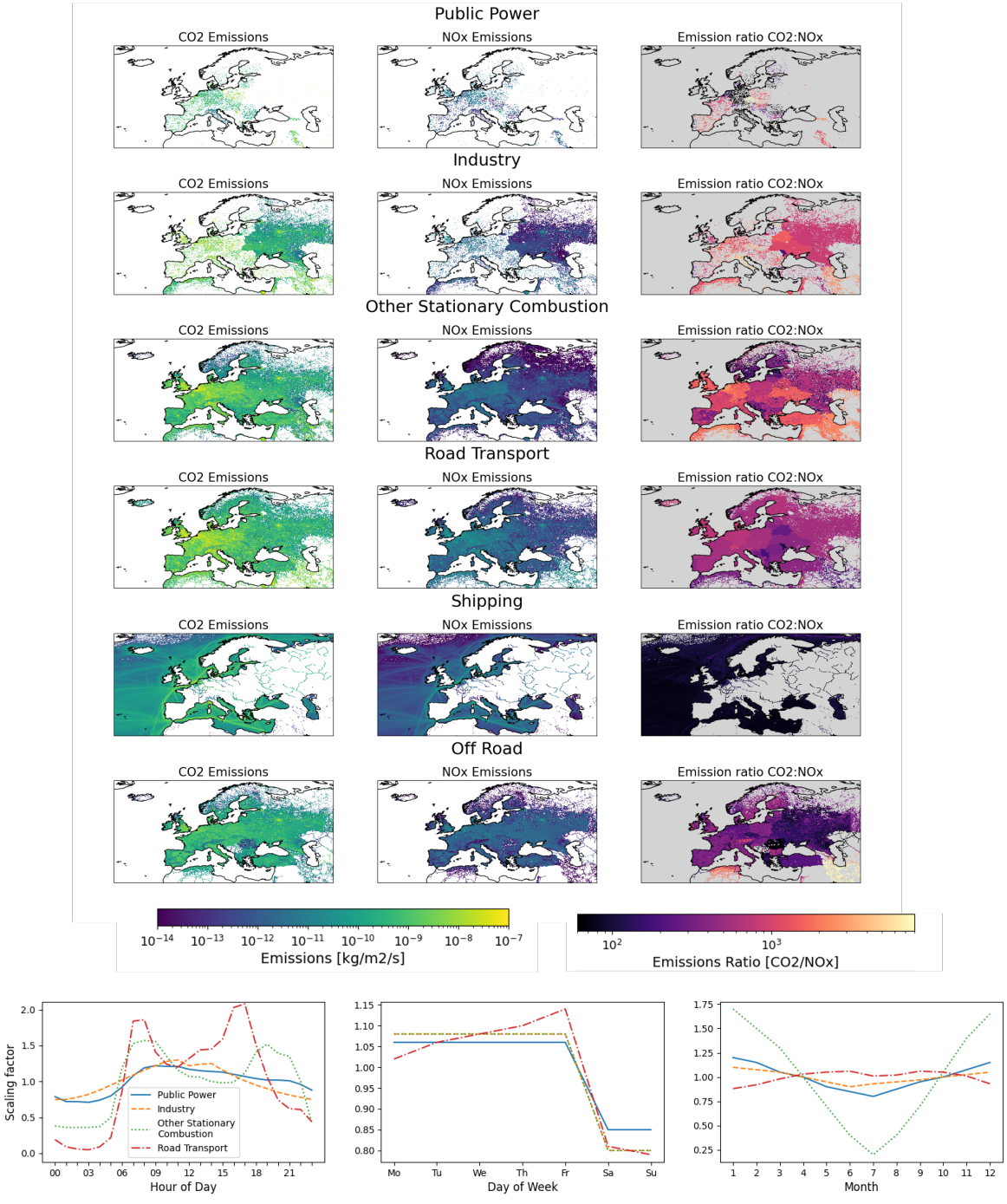

Figure 2. CAMS-REG v8.1 2021 emissions. CO_2 and NO_x with their ratio for six main combustion sectors (top) and temporal profiles for Public Power, Industry, Other Stationary Combustion, and Road Transport (bottom).

https://doi.org/10.5194/egusphere-2026-1315
Preprint. Discussion started: 8 April 2026

from non-combustion sources in the CAMS-REG v8.1 inventory —which include fugitives, waste, solvents, and agriculture — are kept fixed at their prior values. We also prescribe NO_x emissions from soil and lightning, which are parameterised within GEOS-Chem (Vinken et al., 2014; Gressent et al., 2016). For non-fossil-fuel CO_2 sources and sinks we use the CarbonTracker Europe High Resolution (CTE-HR) inventory (van der Woude, 2022), which combines the SiB4 biosphere model v4.2-COS for net ecosystem production (NEP), GFAS fire emissions, and Jena CarboScope ocean fluxes at a 0.5°x0.5° resolution.

To efficiently and effectively incorporate NO_x into our model, we use the methodology presented in Schooling et al. (2025). In that work, we found that for unchanged meteorological conditions but varying emissions, the instantaneous NO_x chemical rates of change can be estimated by scaling the baseline (unperturbed, or prior) rate of change, $R^B(x,y,z,t)$ by the relative change in local NO_x concentration, $[NO_x]'/[NO_x]^B$, where $[NO_x]'$ is the new concentration and $[NO_x]^B$ is the baseline. This reproduces the NO_x chemical rates of change with high fidelity (R^2=1.0). We use the GEOS-Chem full-chemistry simulation to generate hourly offline fields for the baseline NO_x concentrations, $[NO_x]^B(x,y,z,t)$] and instantaneous NO_x net chemistry rates, $R^B(x,y,z,t)$.

For all additional model runs within the data assimilation procedure, we use the carbon model, where NO_x was introduced as a new tracer species. We read in these offline fields and calculate the updated NO_x chemistry net rate of change, $R'(x,y,z,t)$ for each grid point (x, y, z) and time step (t):

$$R'(x,y,z,t) = R^B(x,y,z,t)\frac{[NO_x]'(x,y,z,t)}{[NO_x]^B(x,y,z,t)}. \quad (1)$$

We include the NOx chemistry into the carbon-only simulation through the Kinetic PreProcessor (KPP) mechanism, which describes the production and decay processes of NO_x using the updated calculated rates of change. Additionally, since the partitioning NO_2:NO_x was found to be stable under emission perturbations (Schooling et al., 2025), we store offline fields of the partitioning ratio at each grid point from full chemistry runs, enabling the conversion of simulated NO_x concentrations to NO_2 columns for comparison with TROPOMI observations.

2.3 Ensemble Kalman Filter

We use an existing EnKF framework that has been widely used to estimate CO_2 and methane fluxes from atmospheric data (Feng et al., 2009; Zhu et al., 2022; Feng et al., 2017; Palmer et al., 2019; Feng et al., 2022; Zhu et al., 2025; Feng et al., 2025). The ensemble approach simplifies the calculation of these matrices by approximating the background error covariance matrix ($\mathbf{P}^f$) through a finite sample of model realisations and avoids the needs to calculate an adjoint model.

We introduce an ensemble of $N = 100$ perturbation states. The ensemble approach represents uncertainty in the state vector using a set of model realisations, from which the ensemble mean and perturbations are used to approximate the background error covariance. In our implementation, we use the EnKF to assimilate satellite observations of NO_2 column ($\mathbf{y}_{\mathrm{obs}}$), to update prior knowledge of our state vector, NO_x emission scaling factors ($\mathbf{x}^f$), resulting in posterior scaling factor estimates ($\mathbf{x}^a$):

$$\mathbf{x}^a = \mathbf{x}^f + \mathbf{K}[\mathbf{y}_{\mathrm{obs}} - H(\mathbf{x}^f)], \quad (2)$$

https://doi.org/10.5194/egusphere-2026-1315
Preprint. Discussion started: 8 April 2026

where H is the observation operator that maps the state vector to observation space, which comprises the GEOS-Chem model to relate changes in NO_x emissions to changes in atmospheric NO_2 with the resulting profiles sampled at the time and location of TROPOMI observations and subsequently convolved with scene-dependent averaging kernels.

K is the Kalman gain matrix and is given by:

$$\mathbf{K} \approx \Delta\mathbf{X}^f (\Delta\mathbf{Y}^f)^T \left[\Delta\mathbf{Y}^f (\Delta\mathbf{Y}^f)^T + \mathbf{R}\right]^{-1}, \tag{3}$$

where $\Delta\mathbf{X}^f$ represents the ensemble of deviations from the prior ensemble mean in state space and $\Delta\mathbf{Y}^f$ represents the corresponding ensemble of deviations in the observation space. These quantities are constructed from the ensemble perturbations of the state vector and their mapped equivalents in observation space.

To reduce the impact of spurious long-range correlations, we applied localisation to the Kalman gain. We compute the distance between each grid cell (d_{ij}) and each valid observation, and apply a Gaussian tapering function $\exp(-d_{ij}/l)$ with a decorrelation length scale $l = 200$ km. This localisation is applied multiplicatively to the Kalman gain, element-wise.

For our study, we define **R** as a diagonal matrix that incorporates satellite retrieval uncertainty using the TROPOMI precision values, and includes a fixed model error of 1×10^{13} molec/cm^2, corresponding to the average reconstruction error of NO_2 columns derived from scaled offline chemistry (Schooling et al., 2025). We also employed an adaptive inflation scheme that increased the observation error covariance by a factor of 10 whenever the absolute value of the innovation surpassed a significant threshold ($|\mathbf{d}| > 1 \times 10^{16}$ molec/cm^2).

The ensemble error covariance is derived using our understanding of the CAMS-REG v8.1 emission uncertainties (Super et al., 2026) as well as the error correlation between the two species. The cross-species error correlation (r) is a global product developed under the CORSO project. It is based on the assumption that the error correlation between NO_x and CO_2 occurs from their shared activity data, whereas the emission factor errors are independent. For each emission sector the uncertainties in the activity data (including spatial disaggregation) and emission factors are estimated from the IPCC guidelines (CO_2) (Eggleston et al., 2006), the EMEP guidebook (NO_x) (Nielsen, 2013) and information on the spatial disaggregation of the global EDGAR emission inventory (European Commission, Joint Research Centre, Institute for Environment and Sustainability, 2012). Since these uncertainties are defined per fuel type, information on the fuel mix per country (BP, 2022) is used to aggregate these uncertainties. A look-up table is created that lists the error correlation as a function of the sectoral uncertainty in activity data and emission factors. The higher the uncertainty in the activity data, the larger the cross-species error correlation.

The ensemble background error covariance matrix ($\mathbf{P}^f$) was constructed using the NO_x and CO_2 flux uncertainties (σ_n, σ_c) together with the cross-species error correlation (r):

$$\boldsymbol{P}^f = \begin{pmatrix} \sigma_n^2 & r\sigma_n\sigma_c \\ r\sigma_n\sigma_c & \sigma_c^2 \end{pmatrix}, \tag{4}$$

https://doi.org/10.5194/egusphere-2026-1315
Preprint. Discussion started: 8 April 2026

where the values of σ_n, σ_c and r are prescribed from the CAMS-REG v8.1 uncertainty estimates and the CORSO cross-species correlation product, and are assumed to be constant in time (i.e. no seasonal dependence). We further assume that emission errors are uncorrelated between grid cells, such that the covariance structure is applied independently at each grid location.

We generate an ensemble of NO_x emission scalings by sampling from a bivariate normal distribution, $\mathcal{N}(0, \mathbf{P}^f)$ at each grid cell. This produces spatially resolved perturbations that preserve both the magnitude of uncertainties and the correlation between NO_x and CO_2 errors (Fig. 3).

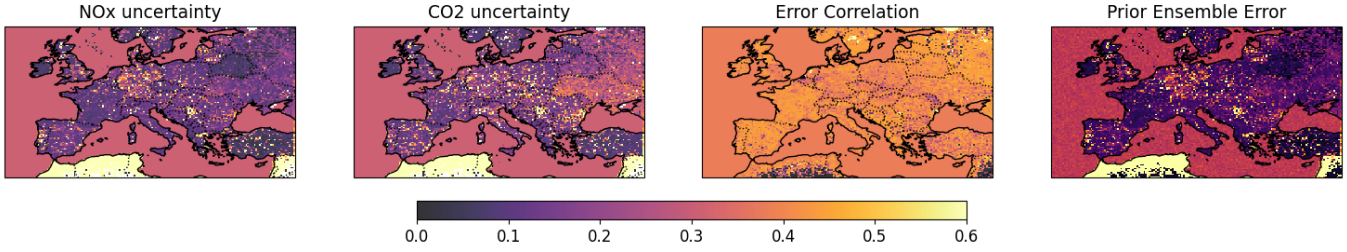

Figure 3. NO_x and CO_2 uncertainties (σ_n, σ_c) from CAMS-REG v8.1 emissions (Super et al., 2026), the cross-species error correlation product (r), taken from the global CORSO product, and the prior ensemble errors calculated from the prior error covariance matrix ($\boldsymbol{P}^f$).

The forward-modelled NO_2 columns from each ensemble member ($H(\mathbf{x}^f)$) are compared to satellite retrievals to compute the innovation vector $\mathbf{d} = \mathbf{y}_{\text{obs}} - H(\mathbf{x}^f)$. We restrict this comparison to grid cells that include valid satellite data (qa>0.75). A spatial mask is applied to exclude edge regions and unphysical retrievals. Edge regions correspond to the outer two GEOS-Chem grid boxes of the domain, and retrievals with NO_2 columns greater than 1×10^{17} molec cm^{-2} are removed as nonphysical.

Since NO_x is short-lived, observations are generally insensitive to emission changes from previous days so we use a data assimilation window of one day. At the end of each assimilation cycle, the posterior emission scaling factors are applied to update the model state through the GEOS-Chem restart file, which is then used to initialise the next day's simulation. Sensitivity tests (Appendix, Fig. A1) show that perturbations introduced through these restart adjustments have a negligible impact on simulated NO_2 columns by the second day, indicating that the observations are primarily sensitive to emission changes occurring within the previous day.

Due to the non-linear relationship between NO_x emissions and atmospheric NO_2, it is possible to maximise error reduction by repeating the ensemble runs multiple times in an iterative data assimilation procedure. Up to four iterations were performed, however the procedure is broken early if the percentage reduction in mean absolute error (MAE) falls below 1%, suggesting a plateau in model improvement.

The posterior flux time series can exhibit relatively strong day-to-day variability, likely driven by gaps and inhomogeneities in the observational coverage that introduce intermittent and uneven constraints within the EnKF system. Additional contributions may arise from underestimated observation or model–data mismatch uncertainties, retrieval artefacts, and transport model errors, which can introduce high-frequency noise into the posterior solution. To reduce this noise and to better isolate robust

https://doi.org/10.5194/egusphere-2026-1315
Preprint. Discussion started: 8 April 2026

temporal signals, we apply a Savitzky–Golay filter to the posterior emission estimates using a 5-day window and a third-order polynomial (Chen et al., 2004).

2.4 Statistical Metrics for Uncertainty and Model Performance

To quantify the reduction in uncertainty within the ensemble we calculate the ensemble-based error reduction (ER):

$$\mathrm{ER} = 100 \times \left(1 - \frac{\sigma_{\mathrm{post}}}{\sigma_{\mathrm{pri}}}\right), \tag{5}$$

where, σ_{pri} and σ_{post} are the prior and posterior ensemble standard deviations, respectively. To quantify the model agreement with observations between our prior and posterior emission estimates, we assess the pearson correlation coefficient (r), the mean bias, and the mean absolute error (MAE).

3 Results

In this section, we report our posterior European NO_x emission estimates and the corresponding $ffCO_2$ estimates for 2021, and the evaluation of the resulting posterior atmospheric NO_2 and CO_2 mole fractions at sites across Europe.

3.1 Inversion results

We find that our inversion leads to a systematic reduction of the state vector uncertainty, with mean ensemble-based Europe-wide error reductions of 5.7%, 4.7%, 4.2%, and 4.6% during DJF, MAM, JJA, and SON, respectively (Fig. 4a). This result demonstrates that TROPOMI NO_2 column data provide effective constraints on NO_x emission estimates, even though we have reasonable bottom-up inventory knowledge.

We note that the larger uncertainty reductions occur over major emission regions such as London, Paris, Madrid – as well as in North Africa, where the prior ensemble spread is highest (Fig. 3). These posterior updates also translate into a general improvement in model minus observation agreement, with an annual increase in pearson r from 0.42 to 0.54, a reduction in mean absolute error of 1×10^{14} molec cm^{-2}, and an overall improvement in the negative bias by 6×10^{13} molec cm^{-2} . Fig. 4b shows the prior and posterior model agreement for each month of the year. The correlation exhibits a marked increase in every month. MAE decreases in all months apart from July, where the prior error was already small, and the negative bias improves in all months apart from May, June, and July, where the prior bias was again already small. Larger posterior adjustments during the colder months likely reflect challenges in bottom-up inventories for domestic heating in winter.

Fig. 5 shows the comparison of the prior and posterior $ffCO_2$ fluxes for Europe in 2021. We find a consistent reduction in emissions uncertainty, from a mean aggregate uncertainty of 5.6% in the prior to 3.3% in the posterior. Our European posterior $ffCO_2$ fluxes exhibit a more pronounced seasonal cycle that found in prior data (Fig. 5a), with larger values during autumn and winter months, most notably during February, November, and December. Conversely, fluxes between mid April and early August remain close to prior values but with a smaller uncertainty.

https://doi.org/10.5194/egusphere-2026-1315
Preprint. Discussion started: 8 April 2026

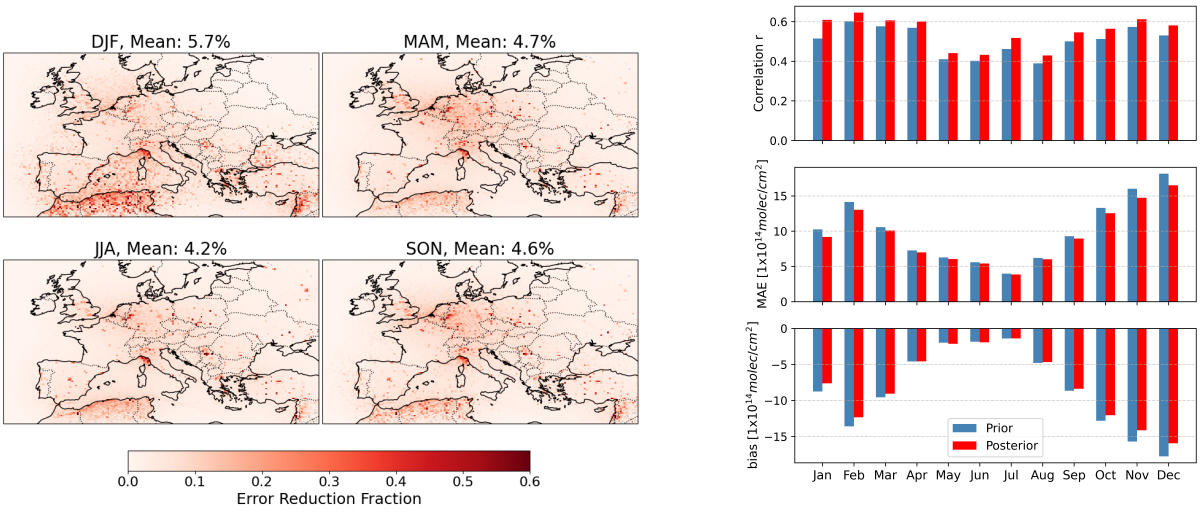

(a) (b)

Figure 4. EnKF inversion performance results. (a) Seasonal maps of the mean ensemble based error reduction (eq. 5). (b) European-wide monthly changes in model performance against TROPOMI NO_2 after posterior flux updates, shown as differences between posterior–observation and prior–observation statistics. Improvements are quantified using pearson r, mean absolute error (MAE), and mean bias.

Fig. 5b shows monthly mean posterior minus prior increments across Europe. Colder months are characterised by widespread increases (10-177% total European daily flux change) relative to the prior while the warmer months show a marked decrease (down to -22% total European daily flux change), particularly over northwestern Europe (United Kingdom, Germany, Netherlands, Belgium), together with some localised increases (Spain, Italy, Turkey).

Fig. 6 shows the national fluxes for 12 high-emitting European countries for 2021 with the corresponding mean surface temperature values derived from the GEOS-FP reanalysis. Generally, we find that individual countries follow the same pattern as the aggregated European total emission trend. Countries that show the most significant and consistent increases in emissions during the colder months include France, Spain, Italy, and Turkey. Reductions in fluxes are observed during some of the summer months in the Netherlands, Belgium, the United Kingdom, and Germany; however, these changes are generally within the range of the prior uncertainty spread.

Across all countries, annual emissions increase relative to the prior, ranging from 20% (United Kingdom) to 91% (Turkey). The change remains below the prior uncertainty (annual change $< 1\sigma$) in the Netherlands, Belgium, and Sweden. In contrast, Spain and Turkey exhibit the largest relative changes, exceeding ten times the prior uncertainty (annual change $> 6\sigma$).

We find a clear negative correlation between our $ffCO_2$ fluxes and local mean temperature, largely reflecting emission peaks during colder winter periods. In February, many countries experienced a considerable number of days with low temperatures, which coincided with a relative increase in emissions. This effect is most pronounced in Sweden, where the mean daily tem-

https://doi.org/10.5194/egusphere-2026-1315
Preprint. Discussion started: 8 April 2026

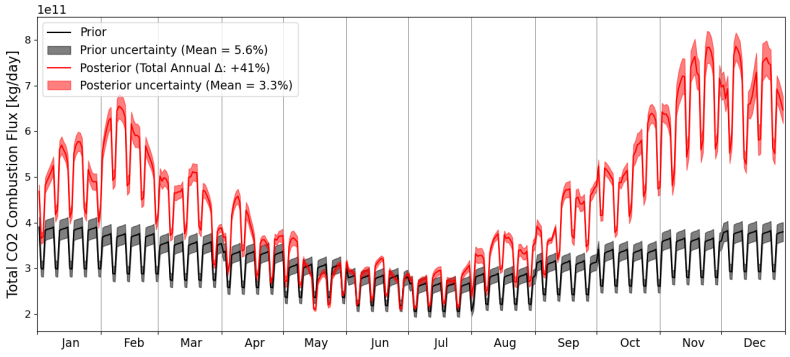

(a)

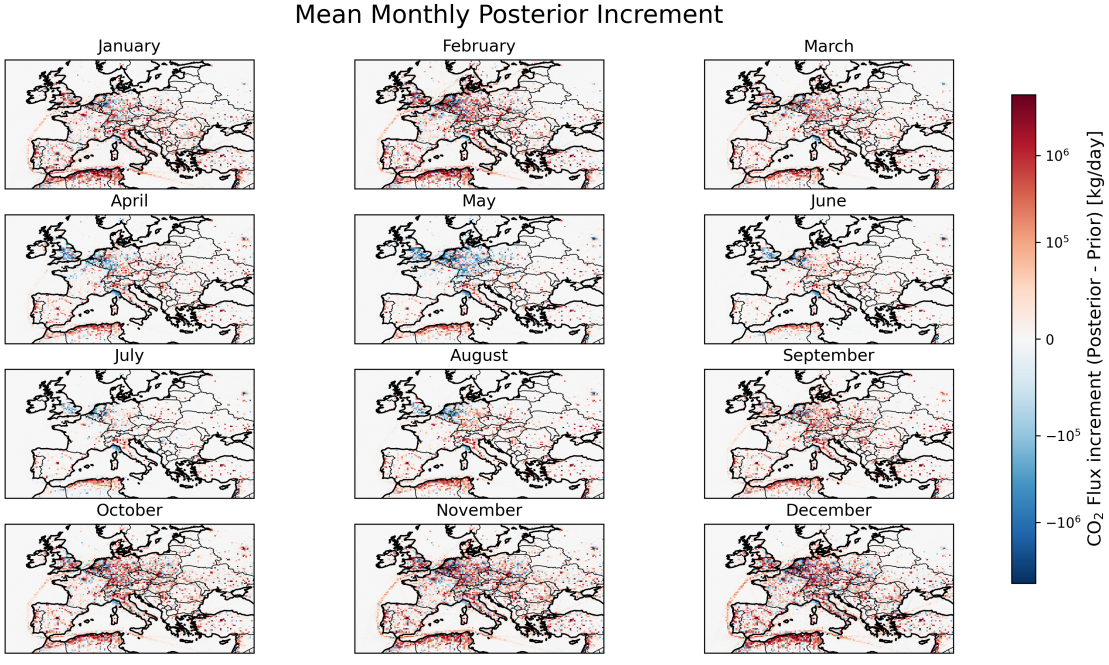

(b)

Figure 5. (a) Full year total European fluxes. Prior fluxes are shown in black with grey uncertainty, and posterior fluxes in red with red shading indicating uncertainity. (b) Mean monthly posterior increment maps show the average regional trends of flux changes (red=increase, blue=decrease relative to prior).

235 perature stayed below $-5°C$ throughout the month, occasionally dropping below $-10°C$, accompanied by a distinct spike in emissions compared to the rest of the year. Similar, though less extreme, cold periods were observed in Germany, the UK, the Netherlands, Belgium, and Turkey, each corresponding to relative emission peaks during February. The posterior $ffCO_2$ shows a strengthened temperature-flux relationship as a consistent increase in the gradient of the correlation between the two variables

https://doi.org/10.5194/egusphere-2026-1315
Preprint. Discussion started: 8 April 2026

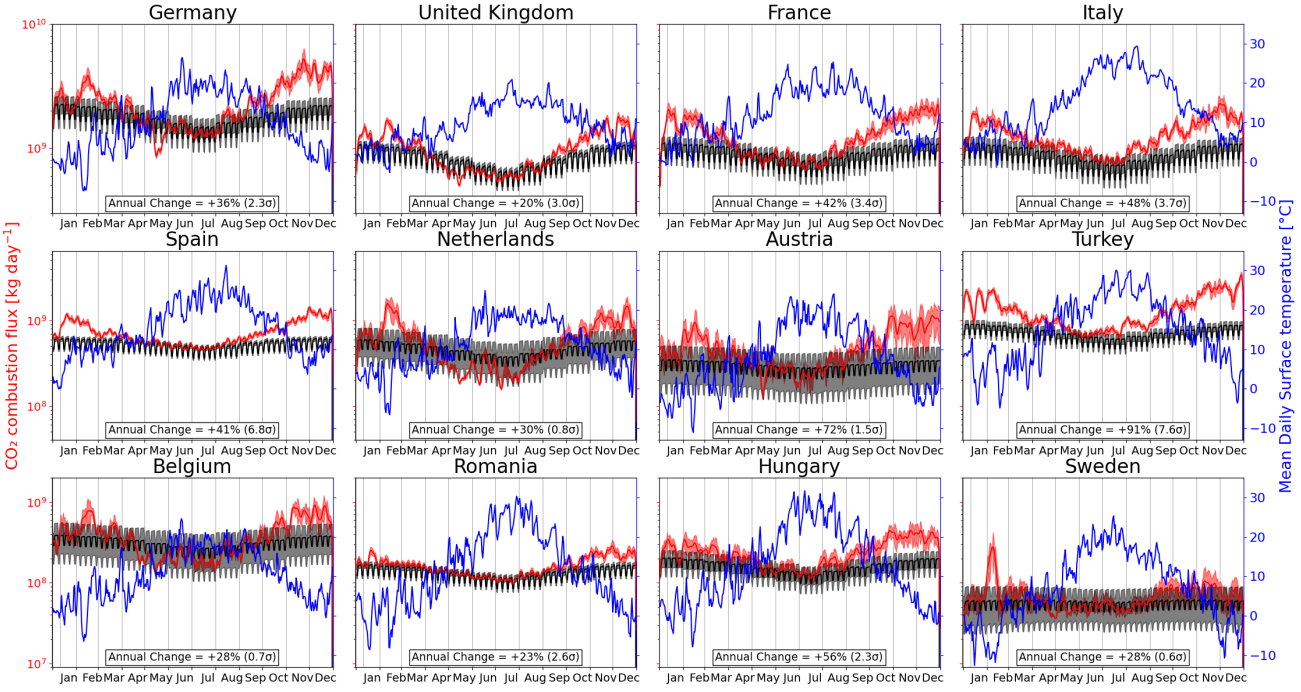

Figure 6. Full year fluxes for 12 high emitting European countries. Prior fluxes are shown in black with grey uncertainty, and posterior fluxes in red with red shading indicating uncertainity (left y-axis). Mean daily temperature is also shown in blue (right y-axis).

(Appendix, Fig. A2). The prior state exhibits two distinct branches, consistent with differing weekday and weekend emission regimes. In the posterior, these merge into a single, more coherent relationship, reflecting a clearer temperature dependence.

3.2 Evaluation of the Posterior Solution

We evaluate our posterior emission estimates of NO_x and $ffCO_2$ by using the GEOS-Chem model as a forward model to calculate the associated atmospheric distributions of NO_2 and CO_2. We compare these posterior atmospheric distributions with in situ NO_2 and CO_2 measurements across Europe and with NASA OCO-2 column observations of CO_2.

Fig. 7 shows the change in model agreement with the EEA in situ NO_2 monitoring network. We find a relatively strong negative bias is present in both the prior and posterior simulations (-18.8, and -16.4 $\mu g/m^3$, respectively). Nevertheless, the posterior values show a clear improvement in correlation, alongside reductions in both MAE and bias. On a monthly basis, MAE decreases in every month of the year, with the largest reductions occurring during the colder months when the posterior flux adjustments are greatest. Correlation improves in all months, but the improvement is most obvious in summer, where prior correlations for June and July were non-existent ($r < 0$) in the prior.

The negative model bias makes sense when we consider that NO_x has a chemical e-folding lifetime of hours to a day, leading to strong spatial gradients and a rapid decay away from emission sources. So that in situ NO_2 measurement sites

https://doi.org/10.5194/egusphere-2026-1315
Preprint. Discussion started: 8 April 2026

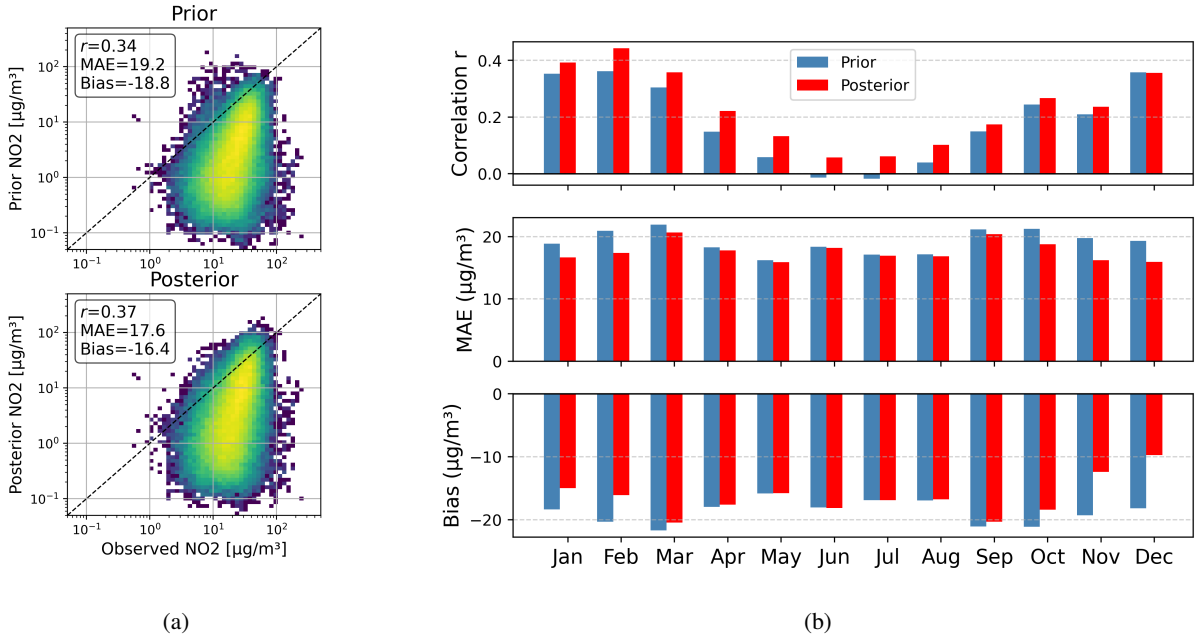

(a) (b)

Figure 7. Model agreement with EEA NO_2 in-situ network. (a) Observed vs. model scatter plots for both the prior and posterior model scenarios. (b) Comparison of prior (blue) and posterior (red) performance metric for each month of the year.

near combustion sources are heavily influenced by local plumes. These plumes exist at a sub-grid scale relative to the GEOS-Chem resolution (0.25° × 0.3125°) and undergo further artificial dilution within the model's lowest surface layer. The model represents a grid-box-mean, vertically averaged concentration that smooths sharp near-source enhancements, and consequently will systematically underestimate point observations.

Fig. 8 and Fig. 9 shows similar a model assessment of posterior atmospheric concentrations but using in situ and OCO-2 column observations of CO_2. Compared with prior values, the posterior CO_2 mole fraction show an overall improvement in agreement with the in situ measurements (Fig. 8a). The month-to-month comparison shows more variability than the NO_2 comparison likely due to additional uncertainties from biogenic fluxes. The correlation improves in all months except June and July. The negative bias is substantially reduced in October, November, and December, supporting the relative increases in posterior fluxes for these months. Conversely, the negative bias at these in situ sites increases in the posterior state during the warmer months (April–September), suggesting that either the posterior increment for CO_2 combustion fluxes should be larger, or that there are inaccuracies in the biogenic uptake in the SiB4 model.

In contrast, the posterior comparison with OCO-2 data shows negligible improvement compared with the prior data. The shifts in correlation and error are an order of magnitude smaller than those seen in the in situ data. This is somewhat to be expected. The columns are much less sensitive to changes in surface emissions than surface in situ data, and variations in OCO-2 CO_2 column data are primarily driven by large-scale biogenic fluxes, which likely mask the relatively small signal contribution

https://doi.org/10.5194/egusphere-2026-1315
Preprint. Discussion started: 8 April 2026

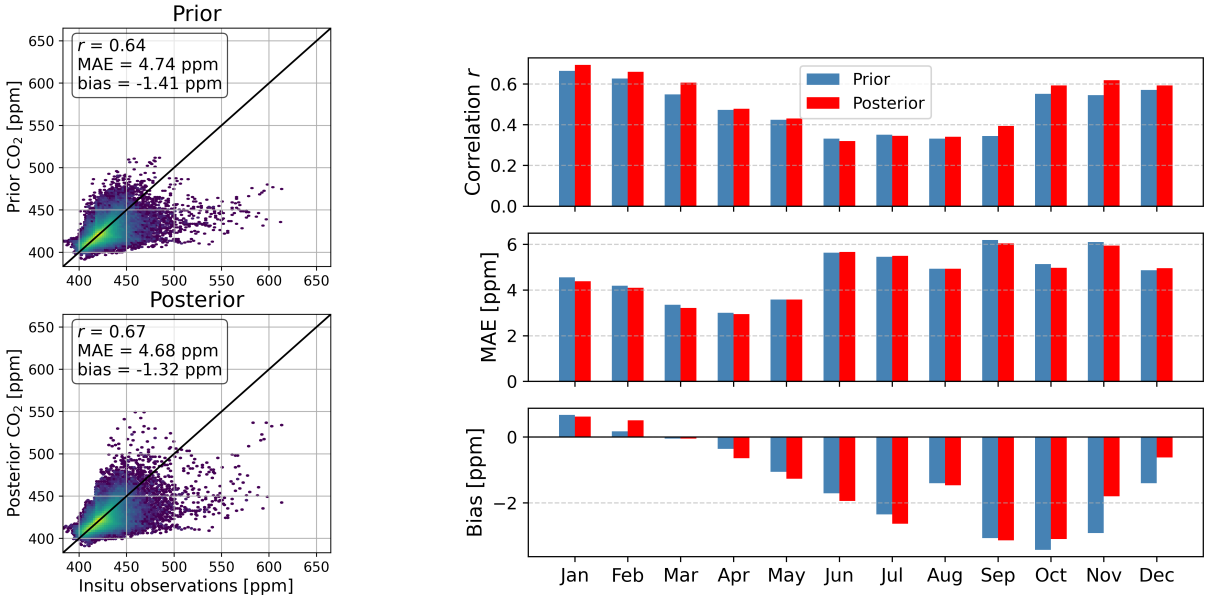

(a) (b)

Figure 8. Model agreement with ICOS, DECC, and NOAA CO_2 in-situ network. (a) Observed vs. model scatter plots for both the prior and posterior model scenarios. (b) Comparison of prior (blue) and posterior (red) performance metric for each month of the year.

from localized ffCO_2 emissions at the column level. Overall, we see a marginal improvement in agreement with the annual data, with the correlation increasing slightly from 0.74 to 0.75. OCO-2 exhibits a positive bias, which is slightly reduced in June and July but worsens in the autumn and winter. Month-to-month correlations show small improvements ($\Delta r > 0.01$) in January, May, September, and December, and negligible changes in remaining months ($|\Delta r| < 0.003$).

4 Concluding remarks

We have presented a satellite-driven ensemble data assimilation framework that utilizes TROPOMI NO2 observations to constrain European NOx and ffCO_2 flux estimates for 2021. By implementing a reduced-complexity NOx chemistry module within GEOS-Chem, we achieved a computationally efficient pathway for multi-species inversions that retains critical chemical feedbacks. This approach reduced posterior flux uncertainty by around 40% (from 5.6% to 3.3%).

Our results reveal a pronounced amplification of the ffCO_2 seasonal cycle—driven by enhanced emissions in autumn and winter—that correlates strongly with surface temperature variability. While independent validation against in situ measurements confirms improved model performance, the limited sensitivity of OCO-2 comparisons highlights the ongoing challenge of isolating fossil fuel signals from large biogenic backgrounds. Ultimately, this study demonstrates that NO_2-driven assimilation provides a robust, spatially resolved constraint on anthropogenic emissions.

https://doi.org/10.5194/egusphere-2026-1315
Preprint. Discussion started: 8 April 2026

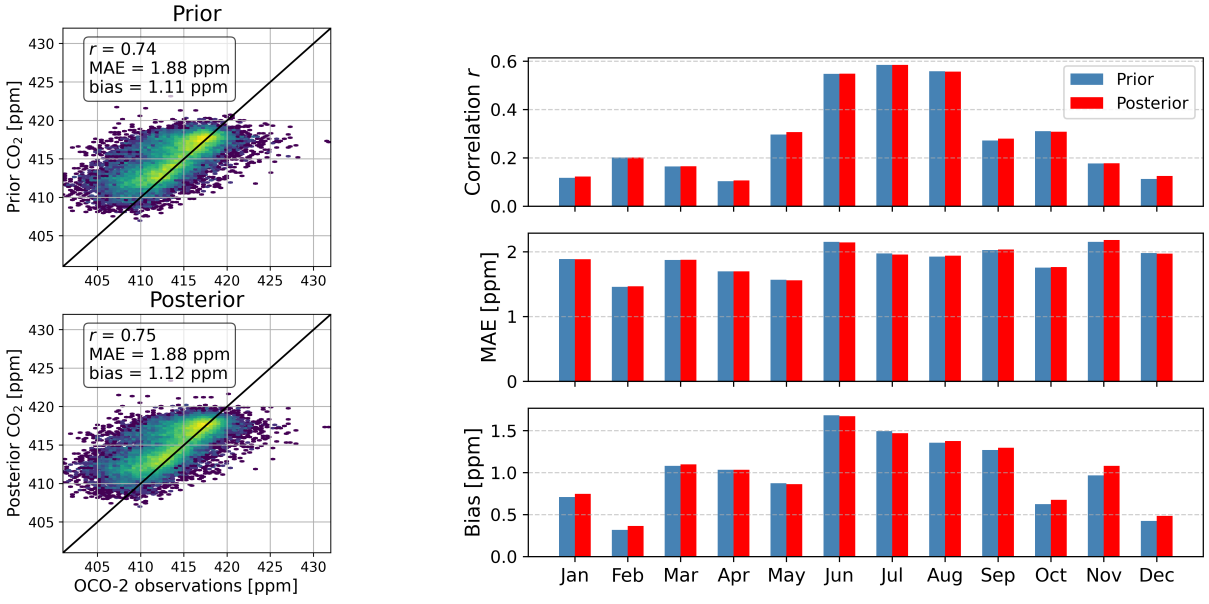

(a) (b)

Figure 9. Model agreement with OCO-2. (a) Observed vs. model scatter plots for both the prior and posterior model scenarios. (b) Comparison of prior (blue) and posterior (red) performance metric for each month of the year.

We acknowledge that our posterior flux adjustments imply substantial increases in national ffCO2 emissions relative to the prior inventory. For all analysed countries the annual total increases by more than 20%, with the largest changes reaching up to 91% in Turkey. These values exceed the stated prior uncertainty in several cases and therefore warrant careful interpretation. While such discrepancies could partly reflect real biases in bottom-up inventories, they may also arise from assumptions within the inversion framework. In particular, the conversion from NOx to ffCO2 emissions relies on prescribed emission ratios that are assumed to be temporally constant. In reality, NOx:CO_2 emission factors will vary across sectors, regions, and seasons due to differences in combustion conditions, fuel composition, and technology (**?**Wang et al., 2025; Super et al., 2020a). A lack of seasonal variability in these emission factors could therefore lead to systematic biases in inferred CO_2 flux adjustments. Future work combining both CO_2 and NO_2 observations within a unified multi-species inversion framework could help better constrain these emission ratios and quantify their seasonal variability, ultimately improving the robustness of satellite-based emission estimates.

Looking forward, the transition toward high-resolution, multi-species satellite constellations necessitates a shift in how we process reactive gas chemistry within carbon-cycle inversions. The success of our reduced-complexity NO_x framework suggests that the historical trade-off between chemical accuracy and computational feasibility is no longer a barrier to operational monitoring. As the Copernicus CO2M mission and GOSAT-GW begin to provide co-located CO_2 and NO_2 retrievals at high spatial and temporal resolution, this ensemble-driven approach can be scaled to provide near-real-time quantification of an-

https://doi.org/10.5194/egusphere-2026-1315
Preprint. Discussion started: 8 April 2026

thropogenic emissions. Future iterations of this system could further refine the NOx-to-CO_2 scaling factors by incorporating sector-specific emission ratios and investigating the impact of diurnal variability in plume chemistry. Ultimately, these advancements will move the community closer to a transparent, satellite-based verification system capable of supporting international climate accords and sub-national emission reduction targets.

5 Code/Data availability

The community-led GEOS-Chem model of atmospheric chemistry and transport is maintained centrally by Harvard University (https://geoschem.github.io/, last access: 10 Feb 2026) and is available on request. The ensemble Kalman filter code is publicly available as PyOSSE (https://www.nceo.ac.uk/data-facilities/datasets-tools//?dataset_type=tools, NCEO, last access: 10 Feb 2026).

6 Author Contributions

C.N.S. and P.I.P. designed the research; I.S. provided NO_x and CO_2 flux uncertainties and error correlations; C.N.S. performed the inversion calculations; C.N.S., L.F., and P.I.P. analysed the results; and C.N.S. and P.I.P. wrote the paper with contributions from L.F. and I.S.

7 Competing Interests

The authors declare that they have no conflict of interest.

8 Acknowledgements

We gratefully acknowledge the GEOS-Chem community, particularly the team at Harvard University who help to maintain the GEOS-Chem model and the NASA Global Modeling and Assimilation Office (GMAO) that provided the MERRA2 data product.

9 Financial support

This research has been supported by the CO2MVS Research on Supplementary Observations (CORSO) project funded by the Horizon Europe programme (grant no. 101082194). L.F. and P.I.P. were also funded by the NERC National Centre for Earth Observation (grant no. NE/R016518/1).

https://doi.org/10.5194/egusphere-2026-1315
Preprint. Discussion started: 8 April 2026

References

Andrew, R. M.: A comparison of estimates of global carbon dioxide emissions from fossil carbon sources, vol. 12, Copernicus Publications Göttingen, Germany, 2020.

Berezin, E. V., Konovalov, I. B., Ciais, P., Richter, A., Tao, S., Janssens-Maenhout, G., Beekmann, M., and Schulze, E.-D.: Multiannual changes of CO_2 emissions in China: indirect estimates derived from satellite measurements of tropospheric NO_2 columns, Atmospheric Chemistry and Physics, 13, 9415–9438, https://doi.org/10.5194/acp-13-9415-2013, 2013.

Bey, I., Jacob, D. J., Yantosca, R. M., Logan, J. A., Field, B. D., Fiore, A. M., Li, Q., Liu, H. Y., Mickley, L. J., and Schultz, M. G.: Global modeling of tropospheric chemistry with assimilated meteorology: Model description and evaluation, Journal of Geophysical Research: Atmospheres, 106, 23 073–23 095, 2001.

BP: Statistical Review of World Energy, Tech. rep., BP p.l.c., https://www.bp.com/content/dam/bp/business-sites/en/global/corporate/pdfs/energy-economics/statistical-review/bp-stats-review-2022-full-report.pdf, accessed: 2026-03-04, 2022.

Chen, J., Jönsson, P., Tamura, M., Gu, Z., Matsushita, B., and Eklundh, L.: A simple method for reconstructing a high-quality NDVI time-series data set based on the Savitzky–Golay filter, Remote Sensing of Environment, 91, 332–344, https://doi.org/10.1016/j.rse.2004.03.014, 2004.

de Foy, B., Lu, Z., Streets, D. G., Lamsal, L. N., and Duncan, B. N.: Estimates of power plant NOx emissions and lifetimes from OMI NO2 satellite retrievals, Atmospheric Environment, 116, 1–11, https://doi.org/https://doi.org/10.1016/j.atmosenv.2015.05.056, 2015.

Eggleston, H., Buendia, L., Miwa, K., Ngara, T., and Tanabe, K.: 2006 IPCC guidelines for national greenhouse gas inventories, 2006.

European Commission, Joint Research Centre, Institute for Environment and Sustainability: Global emission inventories in the Emission Database for Global Atmospheric Research (EDGAR): Manual (I) Gridding: EDGAR emissions distribution on global gridmaps, Publications Office of the European Union, Luxembourg, https://doi.org/10.2788/81454, 2012.

European Environment Agency and Heisig, J.: EEA Air Quality In-Situ Measurement Station Data, https://doi.org/10.5281/ZENODO.17085064, 2025.

Feng, L., Palmer, P. I., Bösch, H., and Dance, S.: Estimating surface CO_2 fluxes from space-borne CO_2 dry air mole fraction observations using an ensemble Kalman Filter, Atmospheric Chemistry and Physics, 9, 2619–2633, https://doi.org/10.5194/acp-9-2619-2009, 2009.

Feng, L., Palmer, P. I., Bösch, H., Parker, R. J., Webb, A. J., Correia, C. S., Deutscher, N. M., Domingues, L. G., Feist, D. G., Gatti, L. V., et al.: Consistent regional fluxes of CH 4 and CO 2 inferred from GOSAT proxy XCH 4: XCO 2 retrievals, 2010–2014, Atmospheric chemistry and physics, 17, 4781–4797, 2017.

Feng, L., Palmer, P. I., Zhu, S., Parker, R. J., and Liu, Y.: Tropical methane emissions explain large fraction of recent changes in global atmospheric methane growth rate, Nature Communications, 13, https://doi.org/10.1038/s41467-022-28989-z, 2022.

Feng, L., Palmer, P. I., Smallman, L., Xiao, J., Cristofanelli, P., Hermansen, O., Lee, J., Labuschagne, C., Montaguti, S., Noe, S. M., Platt, S. M., Ren, X., Steinbacher, M., and Xueref-Remy, I.: The role of the tropical carbon balance in determining the large atmospheric CO 2 growth rate in 2023, Atmospheric Chemistry and Physics, 25, 13 053–13 076, https://doi.org/10.5194/acp-25-13053-2025, 2025.

Goldberg, D. L., Lu, Z., Oda, T., Lamsal, L. N., Liu, F., Griffin, D., McLinden, C. A., Krotkov, N. A., Duncan, B. N., and Streets, D. G.: Exploiting OMI NO2 satellite observations to infer fossil-fuel CO2 emissions from U.S. megacities, The Science of the total environment, 695, 133 805–133 805, 2019.

https://doi.org/10.5194/egusphere-2026-1315
Preprint. Discussion started: 8 April 2026

Goldberg, D. L., Tao, M., Kerr, G. H., Ma, S., Tong, D. Q., Fiore, A. M., Dickens, A. F., Adelman, Z. E., and Anenberg, S. C.: Evaluating the spatial patterns of U.S. urban NOx emissions using TROPOMI NO2, Remote Sensing of Environment, 300, 113 917, https://doi.org/https://doi.org/10.1016/j.rse.2023.113917, 2024.

Gressent, A., Sauvage, B., Cariolle, D., Evans, M., Leriche, M., Mari, C., and Thouret, V.: Modeling lightning-NO_x chemistry on a sub-grid scale in a global chemical transport model, Atmospheric Chemistry and Physics, 16, 5867–5889, https://doi.org/10.5194/acp-16-5867-2016, 2016.

Gu, D., Wang, Y., Smeltzer, C., and Boersma, K. F.: Anthropogenic emissions of NOx over China: Reconciling the difference of inverse modeling results using GOME-2 and OMI measurements, Journal of geophysical research. Atmospheres, 119, 7732–7740, 2014.

Horálek, J., Vlasáková, L., Schreiberová, M., Marková, J., Schneider, P., Kurfürst, P., Tognet, F., Schovánková, J., Vlcek, O., and Damasˇková, D.: European air quality maps for 2020, PM10, PM2, 5, 2023.

ICOS RI, Apadula, F., Arnold, S., Bergamaschi, P., Biermann, T., Chen, H., Colomb, A., Conil, S., Couret, C., Cristofanelli, P., De Mazière, M., Delmotte, M., Di Iorio, T., Emmenegger, L., Forster, G., Frumau, A., Harris, E., Haszpra, L., Hatakka, J., Heliasz, M., Heltai, D., Hensen, A., Hermansen, O., Hoheisel, A., Kneuer, T., Komínková, K., Kubistin, D., Larmanou, E., Laurent, O., Laurila, T., Lehner, I., Lehtinen, K., Leskinen, A., Leuenberger, M., Levula, J., Lindauer, M., Lopez, M., Lund Myhre, C., Lunder, C., Mammarella, I., Manca, G., Manning, A., Marek, M. V., Marklund, P., Meinhardt, F., Miettinen, P., Molnár, M., Montaguti, S., Mölder, M., Müller-Williams, J., O'Doherty, S., Ottosson-Löfvenius, M., Piacentino, S., Pichon, J.-M., Pitt, J., Platt, S. M., Plaß-Dülmer, C., Ramonet, M., Rivas-Soriano, P., Roulet, Y.-A., Scheeren, B., Schmidt, M., Schumacher, M., Sferlazzo, D., Sha, M. K., Smith, P., Stanley, K., Steinbacher, M., Sørensen, L. L., Trisolino, P., Vítková, G., Ylisirniö, A., Yver-Kwok, C., Zazzeri, G., Zwerschke, E., di Sarra, A., ICOS ATC-Laboratoires des Sciences du Climat et de L'Environnement (LSCE), France, ICOS Central Radiocarbon Laboratory (CRL), Germany, and ICOS Flask And Calibration Laboratory (FCL), Germany: ICOS Atmosphere Release 2025-1 of Level 2 Greenhouse Gas Mole Fractions of CO2, CH4, N2O, CO, meteorology and 14CO2, and flask samples analysed for CO2, CH4, N2O, CO, H2, SF6, delta 13C CO2, delta18OCO2, delta O2N2 and 14C, https://doi.org/10.18160/PP29-9CNZ, 2025.

Itahashi, S., Yumimoto, K., Kurokawa, J.-i., Morino, Y., Nagashima, T., Miyazaki, K., Maki, T., and Ohara, T.: Inverse estimation of NOx emissions over China and India 2005-2016: contrasting recent trends and future perspectives, Environmental research letters, 14, 124 020–, 2019.

Jacobs, N., O'Dell, C. W., Taylor, T. E., Logan, T. L., Byrne, B., Kiel, M., Kivi, R., Heikkinen, P., Merrelli, A., Payne, V. H., and Chatterjee, A.: The importance of digital elevation model accuracy in X_{CO_2} retrievals: improving the Orbiting Carbon Observatory 2 Atmospheric Carbon Observations from Space version 11 retrieval product, Atmospheric Measurement Techniques, 17, 1375–1401, https://doi.org/10.5194/amt-17-1375-2024, 2024.

Jia, Y., Tao, M., Zhang, H., Ma, P., Zhao, B., Li, R., Yin, D., Zhang, L., Huang, H., Wang, L., et al.: Estimating Daily NOx and CO2 Emissions in Typical Megacities of East China Using TROPOMI NO2 observations, Atmospheric Environment, p. 121377, 2025.

Jiang, X., Huang, X., Liu, J., and Han, X.: NOx emission of fine-and superfine-pulverized coal combustion in O2/CO2 atmosphere, Energy & fuels, 24, 6307–6313, 2010.

Kaminski, T., Scholze, M., Rayner, P., Houweling, S., Voßbeck, M., Silver, J., Lama, S., Buchwitz, M., Reuter, M., Knorr, W., et al.: Assessing the Impact of Atmospheric CO2 and NO2 Measurements From Space on Estimating City-Scale Fossil Fuel CO2 Emissions in a Data Assimilation System, Frontiers in Remote Sensing, 3, 887 456, 2022.

https://doi.org/10.5194/egusphere-2026-1315
Preprint. Discussion started: 8 April 2026

Kong, Y., Zheng, B., and Liu, Y.: Tracking daily NO_x emissions from an urban agglomeration based on TROPOMI NO_2 and a local ensemble transform Kalman filter, Atmospheric Chemistry and Physics, 25, 5959–5976, https://doi.org/10.5194/acp-25-5959-2025, 2025.

Kuenen, J., Dellaert, S., Visschedijk, A., Jalkanen, J.-P., Super, I., and Denier van der Gon, H.: CAMS-REG-v4: a state-of-the-art high-resolution European emission inventory for air quality modelling, Earth System Science Data, 14, 491–515, 2022.

Kuhlmann, G., Henne, S., Meijer, Y., and Brunner, D.: Quantifying CO2 Emissions of Power Plants With CO2 and NO2 Imaging Satellites, Frontiers in remote sensing, 2, 2021.

Lopez, M., Schmidt, M., Delmotte, M., Colomb, A., Gros, V., Janssen, C., Lehman, S. J., Mondelain, D., Perrussel, O., Ramonet, M., Xueref-Remy, I., and Bousquet, P.: CO, NOx and (CO2)-C-13 as tracers for fossil fuel CO2: results from a pilot study in Paris during winter 2010, Atmospheric chemistry and physics, 13, 7343–7358, 2013.

Meijer, H., Smid, H., Perez, E., and Keizer, M.: Isotopic characterisation of anthropogenic CO2 emissions using isotopic and radiocarbon analysis, Physics and Chemistry of the Earth, 21, 483–487, 1996.

Miyazaki, K. and Bowman, K.: Predictability of fossil fuel CO2 from air quality emissions, Nature Communications, 14, https://doi.org/10.1038/s41467-023-37264-8, 2023.

Nielsen, O.-K.: EMEP/EEA air pollutant emission inventory guidebook 2013. Technical guidance to prepare national emission inventories, 2013.

NOAA Global Monitoring Laboratory, C. C. and Group, G. G.: Continuous In-Situ Measurements of CO_2 at Baseline Sites and Tall Towers (1973–Present), https://doi.org/10.15138/yaf1-bk21, 2025.

Palmer, P. I., Suntharalingam, P., Jones, D. B. A., Jacob, D. J., Streets, D. G., Fu, Q., Vay, S. A., and Sachse, G. W.: Using CO2:CO correlations to improve inverse analyses of carbon fluxes, Journal of Geophysical Research: Atmospheres, 111, https://doi.org/10.1029/2005jd006697, 2006.

Palmer, P. I., Feng, L., Baker, D., Chevallier, F., Bösch, H., and Somkuti, P.: Net carbon emissions from African biosphere dominate pan-tropical atmospheric CO2 signal, Nature communications, 10, 3344, 2019.

Peylin, P., Law, R., Gurney, K., Chevallier, F., Jacobson, A., Maki, T., Niwa, Y., Patra, P., Peters, W., Rayner, P., et al.: Global atmospheric carbon budget: results from an ensemble of atmospheric CO 2 inversions, Biogeosciences, 10, 6699–6720, 2013.

Plauchu, R., Fortems-Cheiney, A., Broquet, G., Pison, I., Berchet, A., Potier, E., Dufour, G., Coman, A., Savas, D., Siour, G., and Eskes, H.: NO_x emissions in France in 2019–2021 as estimated by the high spatial resolution assimilation of TROPOMI NO_2 observations, EGUsphere, 2024, 1–34, https://doi.org/10.5194/egusphere-2024-103, 2024.

Qu, Z., Henze, D. K., Capps, S. L., Wang, Y., Xu, X., Wang, J., and Keller, M.: Monthly top-down NOx emissions for China (2005–2012): A hybrid inversion method and trend analysis, Journal of geophysical research. Atmospheres, 122, 4600–4625, 2017.

Qu, Z., Henze, D. K., Cooper, O. R., and Neu, J. L.: Impacts of global NOx inversions on NO2 and ozone simulations, Atmospheric chemistry and physics, 20, 13 109–13 130, 2020.

Santaren, D., Hakkarainen, J., Kuhlmann, G., Koene, E., Chevallier, F., Ialongo, I., Lindqvist, H., Nurmela, J., Tamminen, J., Amorós, L., Brunner, D., and Broquet, G.: Benchmarking data-driven inversion methods for the estimation of local CO2 emissions from synthetic satellite images of XCO2 and NO2, Atmospheric measurement techniques, 18, 211–239, 2025.

Schooling, C. N., Palmer, P. I., Visser, A., and Bousserez, N.: Development of a parametrised atmospheric NO x chemistry scheme to help quantify fossil fuel CO 2 emission estimates, EGUsphere, 2025, 1–27, 2025.

https://doi.org/10.5194/egusphere-2026-1315
Preprint. Discussion started: 8 April 2026

Schwandner, F. M., Gunson, M. R., Miller, C. E., Carn, S. A., Eldering, A., Krings, T., Verhulst, K. R., Schimel, D. S., Nguyen, H. M., Crisp, D., O'Dell, C. W., Osterman, G. B., Iraci, L. T., and Podolske, J. R.: Spaceborne detection of localized carbon dioxide sources, Science, 358, https://doi.org/10.1126/science.aam5782, 2017.

Stanley, K. M., Grant, A., O'Doherty, S., Young, D., Manning, A. J., Stavert, A. R., Spain, T. G., Salameh, P. K., Harth, C. M., Simmonds, P. G., Sturges, W. T., Oram, D. E., and Derwent, R. G.: Greenhouse gas measurements from a UK network of tall towers: technical description and first results, Atmospheric Measurement Techniques, 11, 1437–1458, https://doi.org/10.5194/amt-11-1437-2018, 2018.

Stavrakou, T., Müller, J.-F., Boersma, K. F., De Smedt, I., and van der A, R. J.: Assessing the distribution and growth rates of NOx emission sources by inverting a 10-year record of NO2 satellite columns, Geophysical research letters, 35, 2008.

Sun, K.: Derivation of Emissions From Satellite-Observed Column Amounts and Its Application to TROPOMI NO2 and CO Observations, Geophysical research letters, 49, 2022.

Suntharalingam, P., Jacob, D. J., Palmer, P. I., Logan, J. A., Yantosca, R. M., Xiao, Y., Evans, M. J., Streets, D. G., Vay, S. L., and Sachse, G. W.: Improved quantification of Chinese carbon fluxes using CO2/CO correlations in Asian outflow, Journal of Geophysical Research: Atmospheres, 109, https://doi.org/10.1029/2003jd004362, 2004.

Super, I., Dellaert, S. N. C., Visschedijk, A. J. H., and Denier van der Gon, H. A. C.: Uncertainty analysis of a European high-resolution emission inventory of CO 2 and CO to support inverse modelling and network design, Atmospheric Chemistry and Physics, 20, 1795–1816, https://doi.org/10.5194/acp-20-1795-2020, 2020a.

Super, I., van der Gon, H. A. C. D., van der Molen, M. K., Dellaert, S. N. C., and Peters, W.: Optimizing a dynamic fossil fuel CO2 emission model with CTDAS (CarbonTracker Data Assimilation Shell, v1.0) for an urban area using atmospheric observations of CO2, CO, NOx, and SO2, Geoscientific Model Development, 13, 2695–2721, 2020b.

Super, I., Mathas, D., Jonkheid, B., Segers, A., and Kuenen, K.: CAMS-REG-UNC-v8.1: A detailed uncertainty product for the gridded CAMS-REG-v8.1 emission inventory, manuscript submitted to Earth System Science Data, 2026.

van der Woude, A.: Near real time fluxes, https://doi.org/10.18160/20Z1-AYJ2, 2022.

van Geffen, J. H. G. M., Eskes, H. J., Boersma, K. F., and Veefkind, J. P.: TROPOMI Algorithm Theoretical Basis Document of the Total and Tropospheric NO_2 Data Products, S5P-KNMI-L2-0005-RP Version 2.4.0, Tech. rep., Royal Netherlands Meteorological Institute (KNMI), De Bilt, The Netherlands, https://sentiwiki.copernicus.eu/__attachments/1673595/S5P-KNMI-L2-0005-RP%20-%20Sentinel-5P%20TROPOMI%20ATBD%20NO2%20data%20products%202022%20-%202.4.0.pdf, accessed: 2025-02-03, 2022.

Veefkind, J. P., Aben, I., McMullan, K., Förster, H., De Vries, J., Otter, G., Claas, J., Eskes, H., De Haan, J., Kleipool, Q., et al.: TROPOMI on the ESA Sentinel-5 Precursor: A GMES mission for global observations of the atmospheric composition for climate, air quality and ozone layer applications, Remote sensing of environment, 120, 70–83, 2012.

Vinken, G. C. M., Boersma, K. F., Maasakkers, J. D., Adon, M., and Martin, R. V.: Worldwide biogenic soil NO_x emissions inferred from OMI NO_2 observations, Atmospheric Chemistry and Physics, 14, 10 363–10 381, https://doi.org/10.5194/acp-14-10363-2014, 2014.

Visser, A. J., Boersma, K. F., Ganzeveld, L. N., and Krol, M. C.: European NOx emissions in WRF-Chem derived from OMI: impacts on summertime surface ozone, Atmospheric chemistry and physics, 19, 11 821–11 841, 2019.

Wang, S., Cohen, J. B., Guan, L., Lu, L., Tiwari, P., and Qin, K.: Observationally constrained global NOx and CO emissions variability reveals sources which contribute significantly to CO2 emissions, npj Climate and Atmospheric Science, 8, 87, 2025.

Wenger, A., Pugsley, K., O'Doherty, S., Rigby, M., Manning, A. J., Lunt, M. F., and White, E. D.: Atmospheric radiocarbon measurements to quantify CO 2 emissions in the UK from 2014 to 2015, Atmospheric Chemistry and Physics, 19, 14 057–14 070, 2019.

https://doi.org/10.5194/egusphere-2026-1315
Preprint. Discussion started: 8 April 2026

Ye, X., Lauvaux, T., Kort, E. A., Oda, T., Feng, S., Lin, J. C., Yang, E. G., and Wu, D.: Constraining Fossil Fuel CO2 Emissions From Urban Area Using OCO-2 Observations of Total Column CO2, Journal of Geophysical Research: Atmospheres, 125, https://doi.org/10.1029/2019jd030528, 2020.

Zhu, S., Feng, L., Liu, Y., Wang, J., and Yang, D.: Decadal methane emission trend inferred from proxy GOSAT XCH4 retrievals: impacts of transport model spatial resolution, Advances in Atmospheric Sciences, 39, 1343–1359, 2022.

Zhu, S., Yang, D., Feng, L., Tian, L., Liu, Y., Cao, J., Zhou, M., Cai, Z., Wu, K., and Palmer, P. I.: Theoretical Potential of TanSat-2 to Quantify China's CH4 Emissions, Remote Sensing, 17, 2321, https://doi.org/10.3390/rs17132321, 2025.

https://doi.org/10.5194/egusphere-2026-1315
Preprint. Discussion started: 8 April 2026

Appendix A

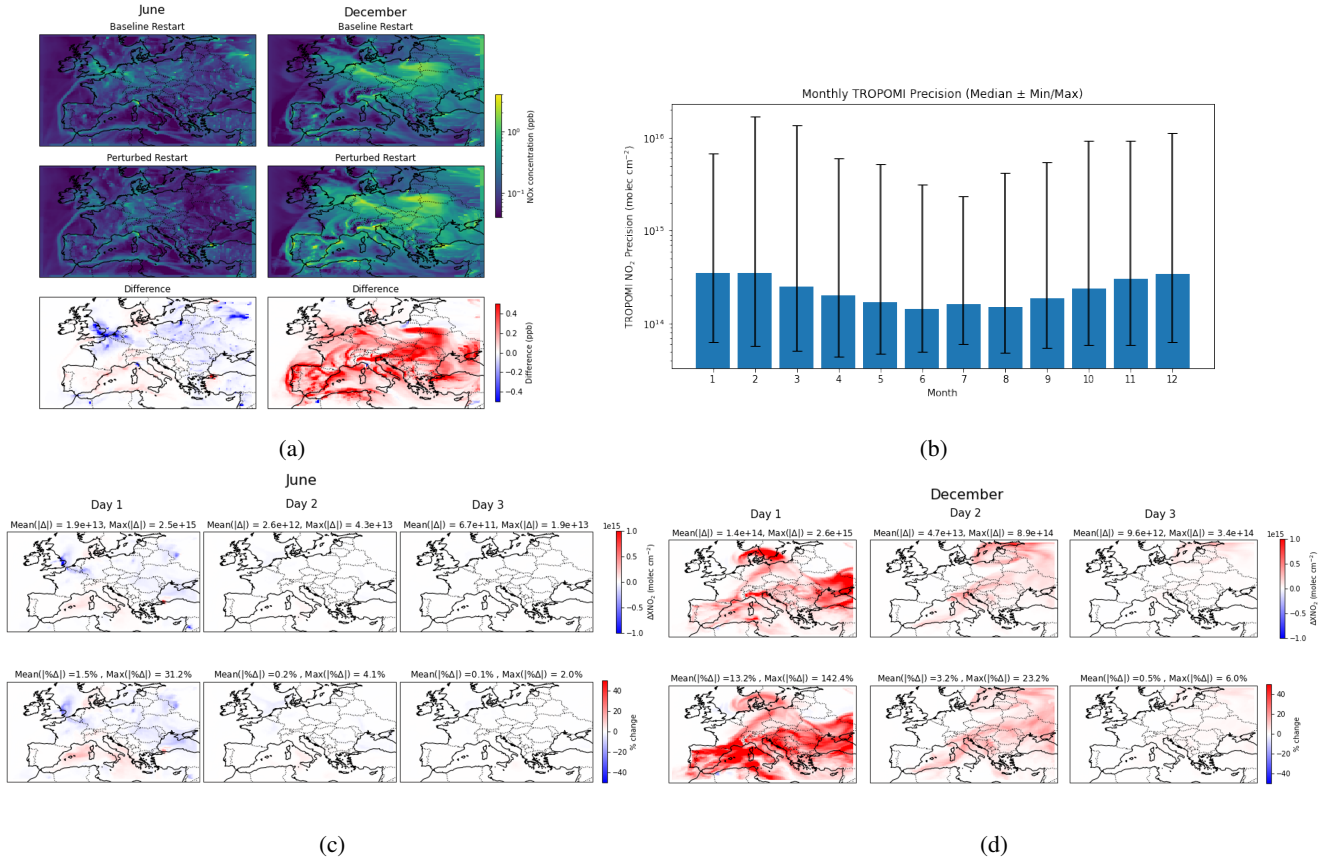

Figure A1. Assessment of modelled XNO_2 column sensitivity to changes in the restart file. (a) Two examples comparing the baseline and perturbed restart files. The June example shows a general decrease in NO_x concentrations in the perturbed state, with small localised increases in the south, whereas the December example shows widespread increases across most of the region. (b) Median and range of TROPOMI precision for each month of 2021. (c, d) Column difference, ΔXNO_2 (molec cm^{-2}) and relative differences (%) between simulations using the two restart files, shown for June (c) and December (d) over days 1, 2, and 3 of the model run. By day 2 in June, the maximum absolute column differences are below TROPOMI precision. In December, by day 2, the mean absolute difference is below, and the maximum absolute difference is comparable to, TROPOMI precision. These results indicate that restart file deviations primarily affect XNO_2 on the first day of the model run, with subsequent days showing changes within or below TROPOMI precision limits.

https://doi.org/10.5194/egusphere-2026-1315
Preprint. Discussion started: 8 April 2026

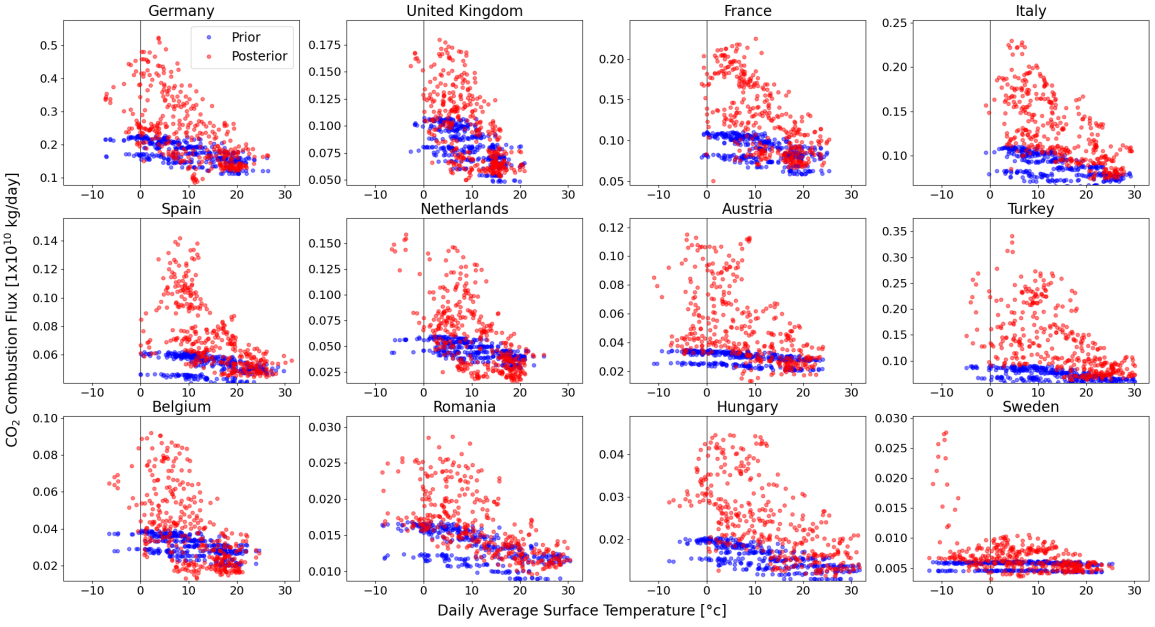

Figure A2. Scatter plots showing the daily average surface temperature against CO_2 combustion fluxes for 12 high emitting countries. The prior fluxes are shown in blue, and the posterior fluxes in red.